Article

Same Precursor, Two Different Products: Comparing the Structural Evolution of In-Ga-O 'Gel-Derived' Powders and Solution-Cast Films using Pair Distribution Function Analysis

Suzannah R Wood, Keenan N. Woods, Paul N. Plassmeyer, David A Marsh, Darren W. Johnson, Catherine J Page, Kirsten M. O. Jensen, and David C. Johnson

J. Am. Chem. Soc., **Just Accepted Manuscript** • DOI: 10.1021/jacs.7b02097 • Publication Date (Web): 22 Mar 2017

Same Precursor, Two Different Products: Comparing the Structural Evolution of In-Ga-O 'Gel-Derived' Powders and Solution-Cast Films using Pair Distribution Function Analysis

Suzannah R. Wood,[†] Keenan N. Woods,[†] Paul N. Plassmeyer,[†] David A. Marsh,[†] Darren W. Johnson,[†] Catherine J. Page,[†] Kirsten M. Ø. Jensen,[‡,*] David C. Johnson[†,*]

†Department of Chemistry and Biochemistry, and Material Science Institute, University of Oregon, Eugene, Oregon, 97403, United States

‡Department of Chemistry, University of Copenhagen, 2100 Copenhagen, Denmark

ABSTRACT: Amorphous metal oxides are central to a variety of technological applications. In particular, indium gallium oxide has garnered attention as a thin-film transistor channel layer material. In this work we examine the structural evolution of indium gallium oxide gel-derived powders and thin films using X-ray diffraction, infrared vibrational spectroscopy, and pair distribution function analysis of X-ray total scattering from standard (PDF) and normal incidence thin film geometries (tfPDF). We find that the gel-derived powders and films from the same aqueous precursor evolve differently with temperature, forming mixtures of Ga-substituted In_2O_3 and In-substituted β-Ga_2O_3 with different degrees of substitution. X-ray total scattering and PDF analysis indicates that the majority phase for both the powders and films is an amorphous/nano-crystalline β-Ga_2O_3 phase, with a minor constituent of In_2O_3 with significantly larger coherence lengths. This amorphous β-Ga_2O_3 phase could not be identified using conventional Bragg diffraction techniques traditionally used to study crystalline metal oxide thin films. The combination of Bragg diffraction and tfPDF provides a much more complete description of film composition and structure, which can be used to detail the effect of processing conditions and structure-property relationships. This study also demonstrates how structural features of amorphous materials, traditionally difficult to characterize by standard diffraction, can be elucidated using tfPDF.

Introduction

Amorphous metal oxide films exhibit a range of attractive properties for technological applications and are candidate materials for next-generation thin-film devices, such as thin-film transistors.[1–11] In particular, amorphous semiconducting oxides such as Zn-O, In_2O_3, amorphous In-Ga-O, amorphous In-Ga-Zn-O, amorphous In-Sn-O, amorphous Zn-In-Sn-O, and amorphous Zn-Sn-O have garnered significant interest.[5,6,9,10] Such materials have been shown to have high electron mobilities,[12,13] tunable conductivity,[14] high optical transparency,[5,6] mechanical stress tolerance,[5,6,15] and compatibility with organic dielectric and photoactive materials,[5] making them applicable for a number of applications.[5,6,11–15] The performance of these materials is strongly correlated with the structure and disorder of the material.[15,16] However, the inherent complexity of amorphous oxide structures has hindered our understanding of chemical transformations and their influence on structure-property relationships.

A variety of approaches have been used to gain insight into the structure of amorphous films, including X-ray reflectivity (XRR),[17–19] ellipsometry,[20] grazing incidence X-ray diffraction (GIXRD),[21] transmission electron microscopy (TEM),[22] electron diffraction,[23] high angle annular dark field-scanning transmission electron microscopy (HAADF-STEM),[24,25] extended X-ray absorption fine structure spectroscopy (EXAFs),[26,27] and solid state nuclear magnetic resonance (ss-NMR).[28,29] Although these traditional techniques provide a variety of structural details, there remains a distinct deficiency in accurately determining the local and mid-range atomic structure of nanostructured materials. X-ray total scattering measurements and pair distribution function analysis have yielded significant structural information about *bulk* amorphous and nanostructured materials, specifically in determining local to long range order.[30–32] However, there has been much less reported using pair distribution function analysis to examine *thin films* on a substrate, due to complicated data analysis procedures and assumptions required about the sample volume and geometry.[8,30] Additionally, in the case of amorphous metal oxides, the low scattering power of O further complicates X-ray structural studies. Because previous experiments on thin films yield only qualitative pair distribution functions (PDF),[30,31] powders made by dehydrating precursor solutions or "gels" have been used as analogues for films.[7,33]

Recently, a normal incidence thin film PDF approach was reported that simplifies the data processing and allows for quantitative analysis of the total scattering data.[32] Here we apply this approach, termed tfPDF, to indium gallium oxide films deposited from aqueous precursor

solutions to understand differences between the structural evolution of 'gel-derived' powders and films. Aqueous solution deposition routes have recently received great interest for their promise of high throughput, low cost production of metal oxide films,[34–38] although little is known about the chemical transformations during processing. We observed several differences in the structures between the gel-derived powder samples, commonly used as a model for films, and film samples. We find that the gel samples crystallize at a lower temperature than the films, and that the composition and coherence length of the crystalline phase formed in the gels is different from that seen in the film samples. Furthermore, we find that for both the gel and film samples, the crystalline phase formed after annealing only constitute a minor phase in the samples, as most of the metal oxide remain in a Ga-rich amorphous phase. These amorphous phases cannot be characterized with conventional diffraction methods, and thus often go unnoticed when coexisting with a crystalline phase. The ability to follow structure evolution of films as a function of annealing temperature enables correlation between the changes in properties and the changes in local, mid, and long range order. This study also highlights the need to study thin film materials directly rather than relying on gel-derived powders as structural analogues.

Experimental

Both the gel-derived powders and thin films were prepared from the same aqueous solutions. $Ga(NO_3)_3 \cdot xH_2O$ (Alfa Aesar, 99.9%) and $In(NO_3)_3 \cdot xH_2O$ (Sigma Aldrich, 99.9%) were dissolved in 18.2 MΩ·cm H_2O for a total metal concentration of 1.5 M (7:6 Ga:In ratio). This solution was filtered through a 0.45 µm syringe filter. The gel-derived powders ("gels") were prepared by rotary evaporation of a solution to dryness and were subsequently annealed in a furnace to specific temperatures, ranging from 200 to 800 °C. For the preparations of thin films, fused silica microslip substrates (Ted Pella, 22x22x0.25 mm) were cleaned using a piranha acid rinse followed by 10 min O_2 plasma etch using a PE-50 Benchtop Plasma Cleaner (Plasma Etch, Inc.) set to maximum power.

Thin films were fabricated by depositing precursor solutions onto cleaned SiO_2 substrates through 0.2 µm PTFE filters. The precursor-coated substrates were then spun at 3000 RPM for 30 seconds and then immediately placed on a preheated hot plate. For films with a final annealing temperature of 200 °C, each layer was heated at 200 °C for 15 min. Layers for all other films were annealed at 300 °C for 5 min. This process was repeated ten times to achieve the desired film thickness. The ten layer films were then ramped at 3.33 °C·min^{-1} to their final annealing temperatures (200, 300, 400, 600, and 800 °C) and held there for 1 h. All spin-coating and annealing was performed under ambient air.

Fourier transform infrared (FTIR) spectroscopy data were collected using a Thermo Scientific Nicolet 6700 FTIR at room temperature. Data from the gel-powder samples were collected in air using an ATR configuration. Data for thin films, deposited on ~2000 Ω·cm Si, were collected in transmission mode in a N_2 environment. All measurements were averaged over 128 spectra, with data spacing of 0.964 cm^{-1}.

GIXRD data on thin film samples were collected using a Rigaku Smartlab (Cu Kα) equipped with parallel beam optics, söller slits, and a scintillation detector using an incident angle of 0.75°. For the gel powder samples, Bragg Brentano diffraction data were collected using a Rigaku Smartlab (Cu Kα) with focused beam optics and a 1-dimensional D/tex Ultra detector. Rietveld refinements were done using *FullProf Suite*.[39]

X-ray total scattering data were collected at room temperature using a wavelength of 0.2114 Å at beamline 11-ID-B of the Advanced Photon Source, Argonne National Laboratory. The gel powder samples were packed into kapton capillaries (1.1 mm inner diameter), and data were collected using the RA-PDF setup.[40] The X-ray total scattering data for the films were collected using the tfPDF technique, where data for both clean substrates and thin films are collected in normal incidence.[32] Pair distribution functions were obtained using PDFgetX3,[41] with Q_{max} = 23.0 Å^{-1}. Real space modeling was done in PDFgui.[42]

Discussion and Results

FTIR spectroscopy highlights chemical differences between thin films (Figure 1a) and gel-derived powders (Figure 1b) annealed at 200, 300, 400, 600, and 800 °C. The IR data allow us to track metal oxide (absorption between 400 and 820 cm^{-1}), nitrate (peaks from ca. 700 to 1100 cm^{-1} and 1200 to 1600 cm^{-1}), water (centered around 1650 cm^{-1}), and hydroxide (peaks between 2900 and 3700 cm^{-1}) content as a function of annealing temperature. For samples annealed at 200 °C, there is a large difference between the gel powder and film sample. While bulk metal nitrates $In(NO_3)_3$ and $Ga(NO_3)_3$ decompose at 240 °C and 224 °C, respectively,[43,44] both persist in gels and films to above 400 °C. The reduced sharpness and number of discernable nitrate absorptions[45,46] and the presence of very broad metal-oxide absorptions from the thin film suggest a higher degree of conversion to the metal oxides and/or hydroxides than for the gel sample. For both gel-derived powder and thin film samples, absorptions from water, hydroxide, and nitrate gradually decrease with increased annealing temperature due to loss of H_2O (1650 cm^{-1}) and condensation reactions between metal hydroxides (2900-3700 cm^{-1}). A gradual evolution of the position and sharpness of the metal-oxide absorptions in the thin-film samples indicates that the bonding arrangements are still changing with annealing temperature. This is in contrast to the powder samples, where the data change very little for samples treated between 300 to 800 °C, which suggests that only small changes to the bonding arrangements occur as annealing temperature increases.

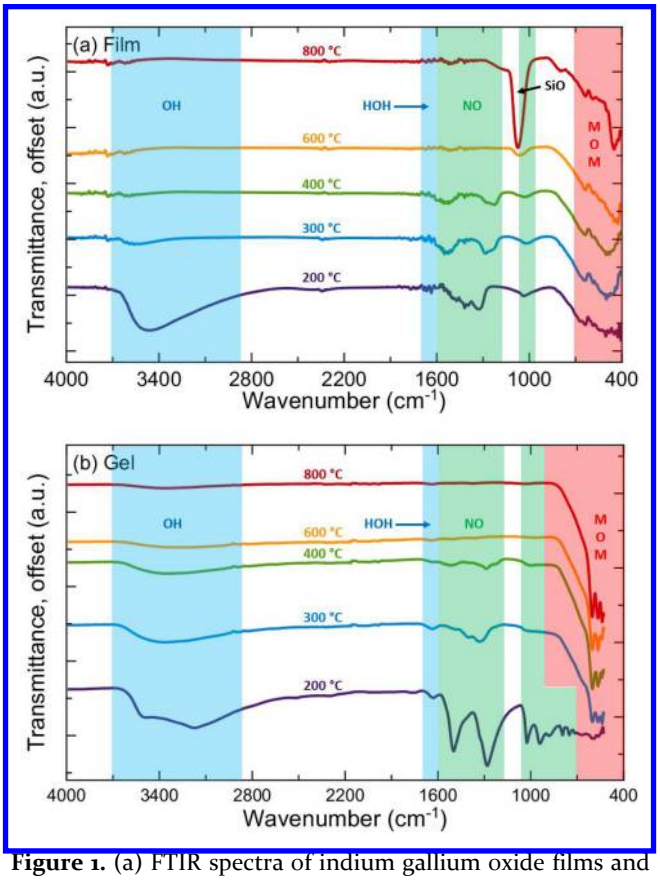

Figure 1. (a) FTIR spectra of indium gallium oxide films and (b) ATR-IR of indium gallium oxide gel powders annealed to various temperatures. The large absorption and shoulder feature, labeled "SiO", around 1025 cm^{-1} is from thermal growth of SiO_2 at the substrate/IGO interface at elevated temperatures.[47]

Figure 2 shows the diffraction patterns of the annealed films and gel-derived powders. The evolution of the scattering pattern with increasing annealing temperature indicates that the crystallization pathways are different in film and gel samples, as seen with IR. GIXRD of the solution-deposited films (Figure 2a) indicates that the films are amorphous at annealing temperatures < 400 °C. Significant differences are seen in the scattering pattern for the samples annealed between 200 and 400 °C indicating large differences in local atomic structure. Weak Bragg peaks from the 600 °C film topping a large background indicate the formation of small crystallites. These Bragg reflections are more apparent in the film annealed at 800 °C. Figure 2b contains powder XRD (PXRD) data for the gel-derived powders, which illustrate that the gels contain crystallites after annealing at 200 °C. The samples annealed at higher temperatures show much more distinct and sharp Bragg peaks, and only slight differences are seen in the diffraction patterns as the gel-derived powder is annealed at higher temperatures. Overall, the gel-derived powder samples have a greater degree of crystallinity and much larger crystallite size than the film samples, which is supported by the intensity of the reflections, the peak full width at half maxima, and the presence of more distinguishable reflections. The PXRD data for the gel-derived powder differ with powder XRD studies on an analogous heterometallic Ga_7In_6 aqueous coordination cluster ($Ga_7In_6(\mu_3\text{-}OH)_6(\mu\text{-}OH)_{18}(H_2O)_{24}(NO_3)_{15}$), which shows a different majority crystalline phase at these temperatures, based on the different location and relative intensities of the Bragg reflections.[48]

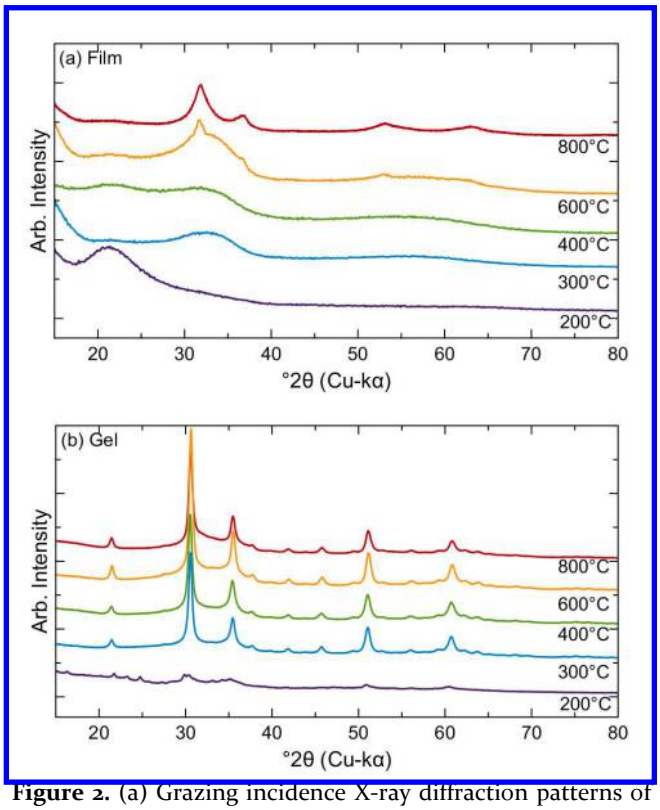

Figure 2. (a) Grazing incidence X-ray diffraction patterns of indium gallium oxide films annealed to various temperatures (b) Bragg-Brentano X-ray diffraction patterns of indium gallium oxide gel-derived powders annealed to various temperatures.

Based on previous investigations in this system, either the In-doped β-Ga_2O_3 phase (C 1 2/m 1) or the $GaInO_3$ (P 63/m m c) phase are expected to crystallize.[48–51] However, the reflections observed are inconsistent with both of these compounds (Figure 3). Instead, the reflections in the diffraction patterns from the crystalline samples can be indexed to a cubic body centered unit cell, which is consistent with a Ga-doped In_2O_3 phase (I a -3).

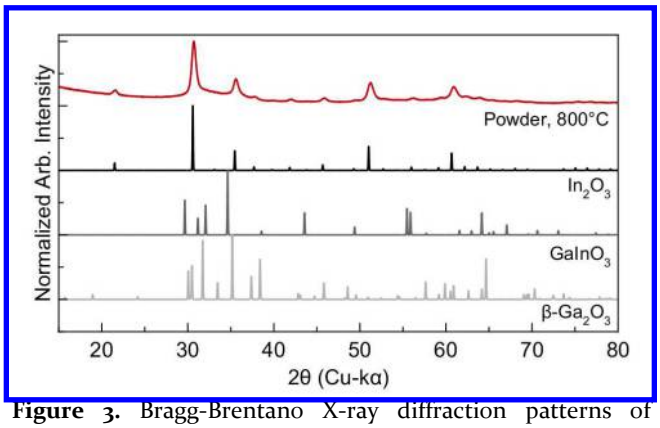

Figure 3. Bragg-Brentano X-ray diffraction patterns of indium gallium oxide gel-derived powder annealed to 800 °C

compared to simulated diffraction patterns for In_2O_3 (I a -3), $GaInO_3$ (P 63/m m c), and β-Ga_2O_3 (C 1 2/m 1).

A least squares fit of the GIXRD data of the film and a Rietveld refinement (Figure 4) of the PXRD data of gel-derived powder showed that the *a* lattice parameter of the film annealed to 800 °C is 9.77(2) Å, while *a* lattice parameter for the gel-derived powder is 10.077(2) Å. A smaller lattice parameter than bulk In_2O_3 (a = 10.117 Å) is consistent with doping with the smaller Ga^{3+} ion for In^{3+} (ionic radii 76 pm and 94 pm, respectively). However, both of these lattice parameters (and that for the film in particular) are significantly smaller than those given in the literature for bulk $(In_{1-x}Ga_x)_2O_3$, which has been reported to form a single phase solid solution only for x < 0.10. The precursor for our samples had a In:Ga ratio of 6:7, corresponding to x = 0.54, assuming 100% reaction yield. The stoichiometry and observed lattice parameters thus suggest that the samples are outside of the homogeneity range reported for the previously prepared bulk phases. Interestingly, nanowires have been prepared with x = 0, 0.11 and 0.25, having lattice parameters of 10.117 Å, 10.100 Å, and 10.094 Å, respectively.[51] Furthermore, the analogous heterometallic Ga_7In_6 aqueous coordination cluster $(Ga_7In_6(\mu_3\text{-}OH)_6(\mu\text{-}OH)_{18}(H_2O)_{24}(NO_3)_{15})$, resulted in a majority phase In-doped β-Ga_2O_3 phase (C 1 2/m 1) and a minority Ga-doped In_2O_3 phase (I a -3) phase. The *a* lattice parameter of the minority phase agrees well with the a-lattice parameter for the gel samples (10.0783(4) and 10.077(2) Å, respectively). Interestingly, the lattice parameters reported in the literature vary considerably from that expected from Vegards law, presumably because the samples are inhomogeneous and overall compositions were used when reporting stoichiometry. This makes the reported homogeneity range somewhat uncertain.

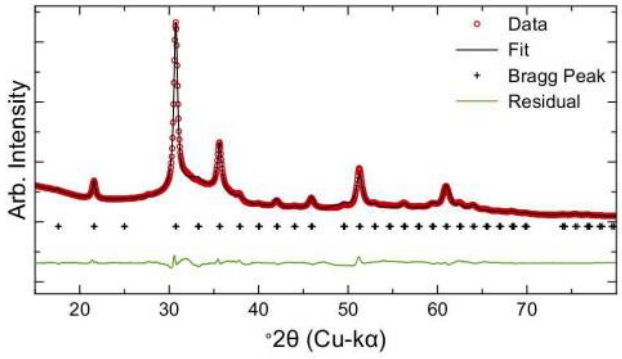

Figure 4. Rietveld refinement of the Bragg-Brentano X-ray diffraction pattern of the indium gallium oxide gel-derived powder annealed to 800 °C.

In the Rietveld refinement, we initially assumed the stoichiometry of the phase to be the same as the precursor solution, i.e. $(In_{0.46}Ga_{0.54})_2O_3$. To test any sensitivity to *x*, refinements with various values were performed. Indeed, the refinement is not very sensitive to the value of *x*, yielding similar refinement quality as *x* is increased at least to 0.65 (Figure S1, Tables S1 and S2). Further characterization is thus needed to explain the lattice parameter observations.

Rietveld refinements were also performed on the gel-derived powder annealed at lower temperatures (Table S3 and Figures S2, S3). The refinements converged to a lattice parameter of 10.085(1), 10.091(1), and 10.102(1) Å for gel-derived powders annealed to 600, 400, and 300 °C, respectively (Figure S2). Interestingly, the decrease in lattice parameter with increasing temperature suggests additional Ga-substitution with increasing temperature in the gel-derived powder samples. This could point to the presence of an amorphous phase, which contains the Ga that is eventually incorporated into the lattice at a higher temperature.

The PXRD data do not allow us to characterize the hypothesized amorphous phase in the gel samples and thus hinders us in understanding the behavior of the unit cell parameter. Furthermore, the low degree of crystallinity and small apparent crystallite size observed for the film samples mean that very limited structural information can be obtained with conventional Bragg diffraction techniques. Therefore, total scattering measurements were conducted to obtain pair distribution functions (PDF) allowing analysis of the local atomic structure (Figure 5) for both films and powders. In the case of the films, the PDF was obtained from the difference of the total scattered intensity of the sample and a measured clean substrate (Figure S4, S5).

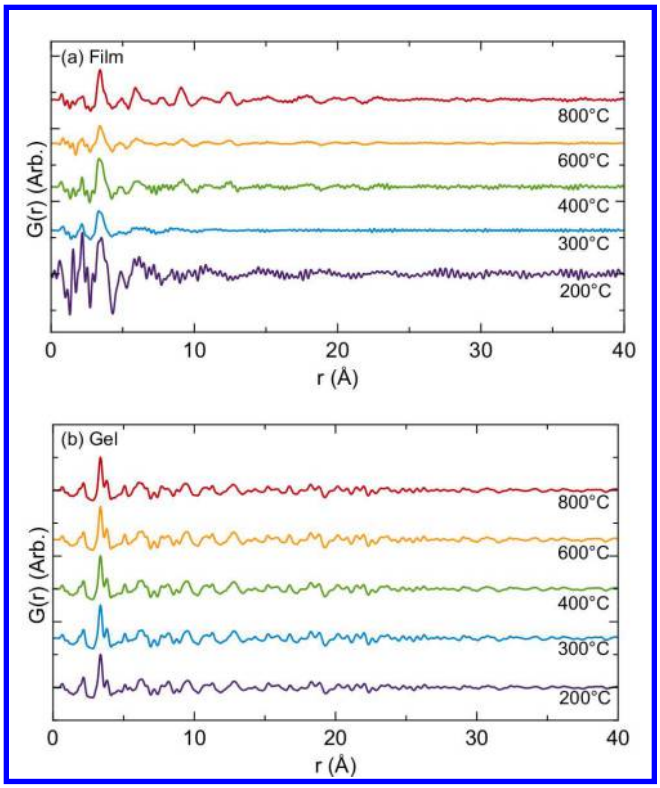

Figure 5. Pair distribution function of indium gallium oxide (a) films and (b) gel derived powders annealed to various temperatures.

In the PDFs of the films (Figure 5a), peaks at higher values of *r* appear with increasing temperature, indicating that structural order in the film increases with increasing

temperature. This is corroborated by the IR and GIXRD data. The PDFs of the gel-derived powder (Figure 5b) have peaks extending to much higher values of *r* at all temperatures, showing significantly more long-range order than the films, as also expected from the PXRD data. Further, they change little with increasing annealing temperature. Even at the lowest annealing temperature investigated (200 °C) the gel-derived powder has long-range order, showing that low temperature nucleation and growth of crystallites occurs in the gels, which agrees well with the FTIR data (Figure 1). Although there are differences in the extent of long-range order, the low r-range of the PDF show that similar atom-atom distances are present in both the gel and film.

The gel-derived powder data were first modeled as a single crystalline phase (Ga-substituted In_2O_3) using the structural model from the Rietveld analysis of the powder data. (Figure 6a). While this model shows relatively good agreement at high *r*-values, fitting the long-range atomic order, large disagreements are seen in the local *r*-range. There is thus a disagreement between the single phase model and the data which is evident in the large residual between 1 and 5 Å (Figure 6a). The disagreement at low *r* indicates the presence of a second component that is amorphous or has a significantly shorter structural coherence length. If considering the difference curve from the fit, significant intensity is seen at 1.89 Å (blue arrow), which is smaller than any metal-oxygen distance in In_2O_3. The gel powder PDF also has significant intensity at 3.35 Å, and a less intense maximum at 3.82 Å (orange and green arrows, Figure 6b), corresponding to the metal-metal distance between the centers of edge sharing (3.35 Å) and corner sharing (3.82 Å) octahedra. In pure, bulk In_2O_3, these maxima in the PDF have equal intensity (Figure S6).

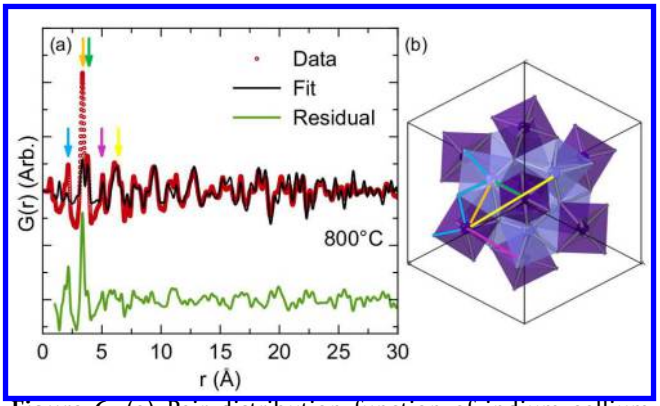

Figure 6. (a) Pair distribution function of indium gallium oxide gel-derived powder annealed 800 °C. Pair distribution functions was fit with (b) crystalline Ga-substituted In_2O_3. Arrows correspond to different atom-atom distances in Ga-substituted In_2O_3, the light and dark polyhedra correspond to the two different metal sites in In_2O_3 and have split In-Ga occupancy.

To explain the difference between the model and data, other possible structures were considered. The calculated PDF of β-Ga_2O_3 contains maxima at 1.89 Å due to Ga-O bonds and its largest maxima at 3.35 Å resulting from Ga-Ga distances. (See Figure S6 for a comparison of theoretical PDFs of In_2O_3 and β-Ga_2O_3 to the gel-derived powder annealed to 800 °C.) This matches well with the unfitted peaks in our data. Additionally, β-Ga_2O_3 was found as a majority phase by Kamunde-Devonish et al., with an analogous In:Ga metal ratio oxide system.[48] We therefore introduced In-doped β-Ga_2O_3 as a second phase in the fit, and allowed a much smaller coherence length than for the main crystalline phase. We were able to fit PDF of the gel annealed at 800 °C using two constituents, 24(3)% of a crystalline Ga-doped $In_2O_3$and 76(3)% of an amorphous phase, whose local structure can be described as In-doped 'β-Ga_2O_3'; these phase percentages result from the least squares fitting of the PDF data. The coherence length ('particle size') refines to 1.3(2) nm (Figure 7, gel 7a). The difference in refined particle sizes explains why we only observe Bragg peaks from the In_2O_3 phase in the gel-derived powder diffraction pattern while the amorphous β-Ga_2O_3 like phase will only give diffuse scattering, seen as a background in the PXRD data (Figure 4). This illustrates how characterization of crystalline fractions of a sample is inadequate, as PXRD only gave information about the minority phase in the system.

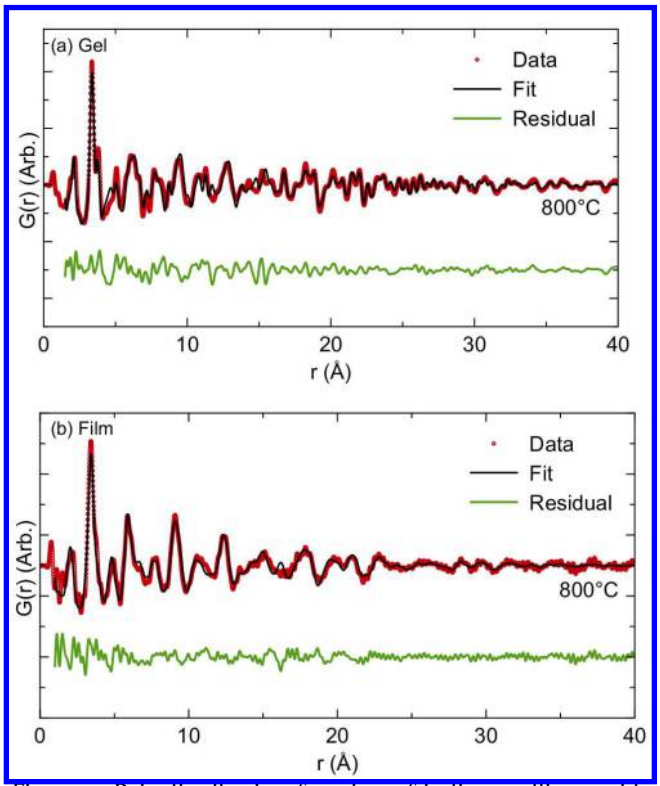

Figure 7. Pair distribution function of indium gallium oxide (a) gel-derived powder and (b) film annealed 800 °C. Pair distribution functions were fit with a mix of crystalline Ga-substituted In2O3 and an amorphous β-Ga2O3 phase as described in the text.

The *a*-axis lattice parameter for the Ga-doped In_2O_3 phase obtained in the PDF fit agrees decently with that obtained from Rietveld refinement of the powder (10.096(5) and 10.077(2), respectively). The lower Q-resolution in RA-PDF measurements means that Rietveld analysis may give a more reliable determination of the

lattice constant. However, comparison of the refined parameters with annealing temperature show that the PDF derived lattice constant shows similar trends as was seen from Rietveld refinements (Figure 8a, Figures S6 – S8 and Tables S4, S5), i.e. a decrease in lattice parameter with annealing temperature. Again, the decrease in *a* indicate larger Ga incorporation at higher temperature. The PDF refinements do indeed show that the fraction of the Ga_2O_3 phase decreases with increasing annealing temperature (Figure 8, Figure S7). The PDF analysis thus explain the behavior of the lattice constant, as Ga is incorporated into the In_2O_3 lattice from the amorphous gallium rich phase during annealing. While additional Ga incorporation at higher temperatures appears to take the system further from the equilibrium phase distribution, the system is not at equilibrium and the phase diagram describes only the equilibrium phase distribution not the kinetics of how the final equilibrium phase distribution is reached. Thus, the system lowers its free energy by forming more crystalline material with a greater Ga incorporation.

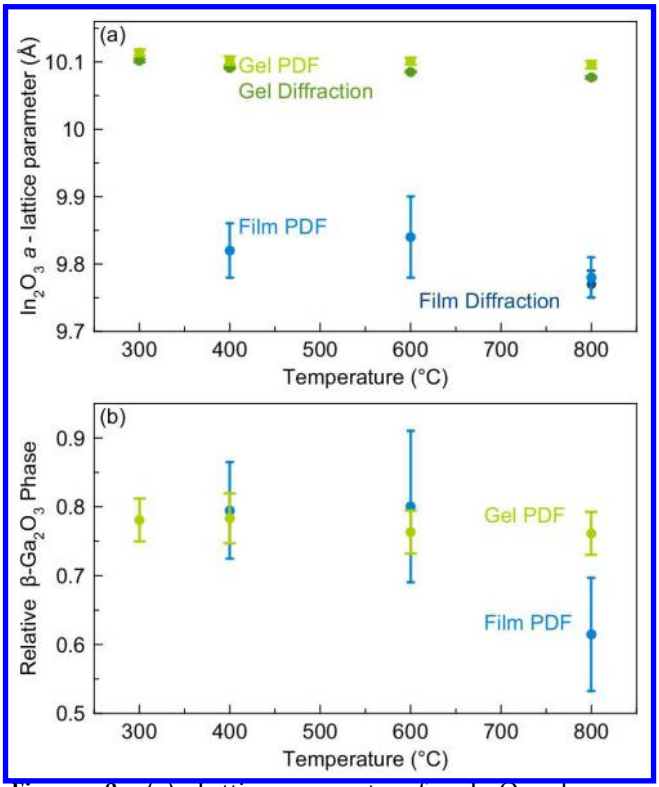

Figure 8. (a) Lattice parameter for In_2O_3 phase as determined by least squares and Rietveld refinements of diffraction and a least squares fit of the pair distribution functions and (b) relative amount of the amorphous β-Ga_2O_3 phase as determined by a least squares fit of the pair distribution functions. The gel-derived powder and film values are shown in green and blue, respectively.

The PDF from the film annealed at 800 °C is shown in Figure 7b. As can be seen on comparison with Figure 5, the film PDF shows a large dependence of the annealing temperature, where increasing structural order is seen with annealing temperature. Just as for the powder samples, the PDF of the film samples could be modeled as the sum of the signals from a crystalline and an amorphous component. Due to the similar local range order, we began with the same structural model as was used for the fit of the gel-data. We were able to fit the PDF of the film at 800 °C using two constituents, 39(8)% of a crystalline Ga-doped In_2O_3 (I a -3) with a particle size of 5(1) nm and 61(8)% of an In-doped β-Ga_2O_3 (C 1 2/m 1) with a particle size of 1.5(4) nm (Figure 7b). The PDF for the film annealed to 400 °C and 600 °C were fit to the same model (Figures S9 – S11 and Tables S6,S7). The percentage of the Ga-doped In_2O_3 phase increases by a factor of two between the 600 °C and 800 °C anneals, explaining the evolution of the thin film diffraction pattern as a function of annealing temperature seen in Figure 2a (Figure 8, Figure S10). The PDFs from films annealed at lower temperatures show shorter correlation lengths (i.e. are completely amorphous), however the metal-oxygen and metal-metal distances are still recognized. For the sample annealed at 200 °C, a peak at 1.9 Å agrees well with a Ga-O bond, 2.16 Å agrees well with a In-O bond, 3.4 Å agrees well with a In-In distance. Unfortunately, the presence of nitrate is difficult to comment on due to the similarity of N-O and Si-O bonds, 1.33 Å and 1.54 – 1.71 Å respectively, complicates the subtraction of the amorphous background.

By combining the results from FTIR, PXRD, and PDF analysis, we gain a new level of insight into the β-Ga_2O_3/In_2O_3 system. For both film and gel samples, we see the presence of both a crystalline and amorphous phases, with the amorphous phase dominating. This illustrates that just characterizing the crystalline part of a sample is not sufficient: Our analysis of the samples suggests that previous results, which indicated that Vegard's law did not hold, should not have used the nominal composition of the sample as the composition for the Ga doped In_2O_3, as a large portion of the Ga/In may be present in amorphous or nanostructured phase. The differences between the film and the gel-derived powder are considerable considering that they were formed from the same precursor solution. While both the gel-derived powder and films resulted in the same structural phases $(In_{1-x}Ga_x)_2O_3$ and an amorphous phase with β-$(Ga_{1-y}In_y)_2O_3$ like structure, the refined lattice constants from PDF analysis and Rietveld refinement indicate that the degree of Ga-substitution into In_2O_3 and In-substitution into β-Ga_2O_3 is different. Both the lattice parameter and the refined phase fractions show that more Ga^{3+} is incorporated into the In_2O_3 phase in the film, which at the same time form much smaller crystallites than for the gels.

We explain these differences by invoking different reaction mechanisms: The spin coating procedure used for film preparation leads to a faster condensation than the happening in the gel samples during the rotary evaporation and following annealing. This can be seen by the metal-oxide absorptions in the IR data. In the gel-derived powders, the atoms were thus able to diffuse and form much larger crystallites than in the more rapidly condensed film, where evaporation and condensation happen at the same time over a much shorter time. The longer time required to evaporate the gel to a dry powder yields a product closer to the thermodynamically stable phase

configuration, as seen by lattice parameters more closely representing the previously reported bulk materials. In contrast, rapid film formation during spin coating limits the time that atoms have to diffuse, and thus form very small nanoparticles with compositions far from the previously reported homogeneity range. Traditional nucleation and growth models would predict that the Ga-doped In_2O_3 crystallites form from the amorphous network. This would result in a morphology wherein Ga-doped In_2O_3 crystallites are embedded within the amorphous matrix. Surprisingly, the gel and film maintain their differences throughout our annealing study, suggesting that even higher temperatures and/or longer reaction times are required to converge to the same product.

CONCLUSIONS

The local, mid, and long range structure of gel-derived powders and thin films of indium gallium oxide made from the same precursor solution were investigated using PDF and a suite of corroborative techniques. The data indicates that processing conditions play a pivotal role in the evolution and crystallization of the aqueous precursor into the mixture of compounds formed. This study highlights the need to study thin film materials as thin films rather than relying on gel-derived powder surrogates, and highlights the utility of tfPDF analysis of the X-ray total scattering data for structural analysis of amorphous films. The tfPDF analysis enabled the structure of amorphous and nanocrystalline films to be followed as a function of processing conditions, which had been previously inaccessible for oxide systems. Furthermore, PDF analysis of both the film and gel samples revealed that the majority of the product is present as an amorphous phase, which cannot be characterized using standard PXRD and may be erroneously ascribed as a background in the diffraction pattern. The ability to use pair distribution analysis on both films and gels thus provides a powerful tool for comparing short, mid, and long range order of these largely amorphous materials. This combination of analytical approaches (Bragg diffraction, IR analysis, total scattering and pair-distribution analysis) is particularly promising for investigating structural evolution in films derived from aqueous inorganic systems, due to the complex solution chemistry that can occur as the system evaporates to dryness. Determination of the evolution of amorphous and crystalline constituents in films is essential to understanding synthetic pathways and, ultimately, will allow for the optimization of the performance of thin-film devices.

ASSOCIATED CONTENT

Supporting Information. Rietveld refinement analysis with fit parameters and PDFgui fits with fit parameters. This material is available free of charge via the Internet at http://pubs.acs.org.

AUTHOR INFORMATION

Corresponding Author

* E-mail: davej@uoregon.edu, kirsten@chem.ku.dk

ACKNOWLEDGMENT

Coauthors SRW, KNW, PNP, DAM, DWJ, DCJ and CJP acknowledge support from the National Science Foundation Center for Sustainable Materials Chemistry grant number CHE-1606982. KMØJ acknowledges funding from the Danish Research Council under the Sapere Aude Research Talent Program
. The authors thank Karena Chapman and Kevin Beyer at 11-ID-B for technical assistance during collection of the synchrotron XRD data. Use of the Advanced Photon Source was supported by the U. S. Department of Energy, Office of Science, Office of Basic Energy Sciences, under Contract No. DE-AC02-06CH11357.

ABBREVIATIONS

PDF, Pair Distribution Function. tfPDF, thin film Pair Distribution Function.

REFERENCES

(1) Choi, J. Y.; Heo, K.; Cho, K.-S.; Hwang, S. W.; Kim, S.; Lee, S. Y. *Sci. Rep.* **2016**, *6*, 36504.
(2) Sharma, V.; Vyas, R.; Bazylewski, P.; Chang, G. S.; Asokan, K.; Sachdev, K. *RSC Adv.* **2016**, *6*, 29135–29141.
(3) Veal, B. W.; Kim, S. K.; Zapol, P.; Iddir, H.; Baldo, P. M.; Eastman, J. A. *Nat. Commun.* **2016**, *7*, 11892.
(4) Taz, H.; Sakthivel, T.; Yamoah, N. K.; Carr, C.; Kumar, D.; Seal, S.; Kalyanaraman, R. *Sci. Rep.* **2016**, *6*, 27869.
(5) Yu, X.; Marks, T. J.; Facchetti, A. *Nat Mater* **2016**, *15*, 383–396.
(6) Yu, X.; Smith, J.; Zhou, N.; Zeng, L.; Guo, P.; Xia, Y.; Alvarez, A.; Aghion, S.; Lin, H.; Yu, J.; Chang, R. P. H.; Bedzyk, M. J.; Ferragut, R.; Marks, T. J.; Facchetti, A. *Proc. Natl. Acad. Sci.* **2015**, *112*, 3217–3222.
(7) Llordes, A.; Wang, Y.; Fernandez-Martinez, A.; Xiao, P.; Lee, T.; Poulain, A.; Zandi, O.; Saez Cabezas, C. A.; Henkelman, G.; Milliron, D. J. *Nat Mater* **2016**, *15*, 1267–1273.
(8) Shyam, B.; Stone, K. H.; Bassiri, R.; Fejer, M. M.; Toney, M. F.; Mehta, A. *Sci. Rep.* **2016**, *6*, 32170.
(9) Mitzi, D. B. *J. Mater. Chem.* **2004**, *14*, 2355.
(10) Fortunato, E.; Barquinha, P.; Martins, R. *Adv. Mater.* **2012**, *24*, 2945–2986.
(11) Nomura, K.; Takagi, A.; Kamiya, T.; Ohta, H.; Hirano, M.; Hosono, H. *Japanese J. Appl. Physics, Part 1 Regul. Pap. Short Notes Rev. Pap.* **2006**, *45*, 4303–4308.
(12) Hosono, H. *J. Non. Cryst. Solids* **2006**, *352*, 851–858.
(13) Robertson, J. *Phys. status solidi* **2008**, *245*, 1026–1032.
(14) Divya; Prasad, R.; Deepak. *Phys. status solidi* **2017**, *1*, 1600471.
(15) Nomura, K.; Ohta, H.; Takagi, A.; Kamiya, T.; Hirano, M.; Hosono, H. *Nature* **2004**, *432*, 488–492.
(16) Martins, R.; Barquinha, P.; Ferreira, I.; Pereira, L.; Gocalves, G.; Fortunato, E. *J. Appl. Phys.* **2007**, *101*, 0–7.
(17) Morelhão, S. L.; Brito, G. E. S.; Abramof, E. *Appl. Phys. Lett.* **2002**, *80*, 407.
(18) Gutmann, E.; Meyer, D. C.; Levin, A. A.; Paufler, P. *Appl. Phys. A Mater. Sci. Process.* **2005**, *81*, 249–259.
(19) Jiang, K.; Meyers, S. T.; Anderson, M. D.; Johnson, D. C.; Keszler, D. a. *Chem. Mater.* **2013**, *25*, 210–214.
(20) Loke, V. L. Y.; Riefler, N.; Mehner, A.; Prenzel, T.; Hoja, T.; Wriedt, T.; Mädler, L. *Thin Solid Films* **2013**, *531*, 93–98.
(21) Nadarajah, A.; Wu, M. Z. B.; Archila, K.; Kast, M. G.; Smith, A. M.; Chiang, T. H.; Keszler, D. A.; Wager, J. F.; Boettcher, S. W. *Chem. Mater.* **2015**, *27*, 5587–5596.
(22) Teodorescu, V. S.; Blanchin, M. G. In *Microscopy: Advances in Scientific Research and Education*; FORMATEX: Madrid, Spain, 2014; 903–910.
(23) Cockayne, D. J. H.; McKenzie, D. R. *Acta Crystallogr. Sect. A Found. Crystallogr.* **1988**, *44*, 870–878.

(24) Fairley, K. C.; Merrill, D. R.; Woods, K. N.; Ditto, J.; Xu, C.; Oleksak, R. P.; Gustafsson, T.; Johnson, D. W.; Garfunkel, E. L.; Herman, G. S.; Johnson, D. C.; Page, C. J. *ACS Appl. Mater. Interfaces* **2016**, *8*, 667–672.

(25) Mitchson, G.; Ditto, J.; Woods, K. N.; Westover, R.; Page, C. J.; Johnson, D. C. *Semicond. Sci. Technol.* **2016**, *31*, 84003.

(26) Sayers, D. E.; Stern, E. A.; Lytle, F. W. *Phys. Rev. Lett.* **1971**, *27*, 1204–1207.

(27) Fuoss, P. H.; Eisenberger, P.; Warburton, W. K.; Bienenstock, A. *Phys. Rev. Lett.* **1981**, *46*, 1537–1540.

(28) Lee, S. K.; Park, S. Y.; Yi, Y. S.; Moon, J. *J. Phys. Chem. C* **2010**, *114*, 13890–13894.

(29) Lee, S. K.; Ahn, C. W. *Sci. Rep.* **2014**, *4*, 4200.

(30) Fischer-Colbrie, A.; Bienenstock, A.; Fuoss, P. H.; Marcus, M. A. *Phys. Rev. B* **1988**, *38*, 388–403.

(31) Rigden, J. S.; Newport, R. J.; Bushnell-Wye, G. *J. Mater. Res.* **2011**, *12*, 264–276.

(32) Jensen, K. M. Ø.; Blichfeld, A. B.; Bauers, S. R.; Wood, S. R.; Dooryhée, E.; Johnson, D. C.; Iversen, B. B.; Billinge, S. J. L. *IUCrJ* **2015**, *2*, 481–489.

(33) Hou, Y.; Fast, D. B.; Ruther, R. E.; Amador, J. M.; Fullmer, L. B.; Decker, S. R.; Zakharov, L. N.; Dolgos, M. R.; Nyman, M. *J. Solid State Chem.* **2015**, *221*, 418–425.

(34) Kast, M. G.; Cochran, E. A.; Enman, L. J.; Mitchson, G.; Ditto, J.; Siefe, C.; Plassmeyer, P. N.; Greenaway, A. L.; Johnson, D. C.; Page, C. J.; Boettcher, S. W. *J. Am. Chem. Soc.* **2016**, *138*, 16800–16808.

(35) Takata, R.; Neumann, A.; Weber, D.; Pham, D.-V.; Anselmann, R.; Kitamura, Y.; Kakimura, T.; Suzuki, S.; Minami, S.; Kodama, M. *J. Soc. Inf. Disp.* **2016**, *24*, 381–385.

(36) Thomas, S. R.; Pattanasattayavong, P.; Anthopoulos, T. D. *Chem. Soc. Rev.* **2013**, *42*, 6910–6923.

(37) Kim, M.-G.; Kanatzidis, M. G.; Facchetti, A.; Marks, T. J. *Nat. Mater.* **2011**, *10*, 382–388.

(38) Kim, H. S.; Kim, M.-G.; Ha, Y.-G.; Kanatzidis, M. G.; Marks, T. J.; Facchetti, A. *J. Am. Chem. Soc.* **2009**, *131*, 10826–10827.

(39) Roisnel, T.; Rodríquez-Carvajal, J. *Mater. Sci. Forum* **2001**, *378–381*, 118–123.

(40) Chupas, P. J.; Qiu, X.; Hanson, J. C.; Lee, P. L.; Grey, C. P.; Billinge, S. J. L. *J. Appl. Crystallogr.* **2003**, *36*, 1342–1347.

(41) Juhás, P.; Davis, T.; Farrow, C. L.; Billinge, S. J. L. *J. Appl. Crystallogr.* **2013**, *46*, 560–566.

(42) Farrow, C. L.; Juhas, P.; Liu, J. W.; Bryndin, D.; Božin, E. S.; Bloch, J.; Proffen, T.; Billinge, S. J. L. *J. Phys. Condens. Matter* **2007**, *19*, 335219.

(43) Xu, W.; Cao, H.; Liang, L.; Xu, J.-B. *ACS Appl. Mater. Interfaces* **2015**, *7*, 14720–14725.

(44) Rim, Y. S.; Chen, H.; Song, T.-B.; Bae, S.-H.; Yang, Y. *Chem. Mater.* **2015**, *27*, 5808–5812.

(45) Rudolph, W. W.; Pye, C. C. *Phys. Chem. Chem. Phys.* **2002**, *4*, 4319–4327.

(46) Rudolph, W. W.; Fischer, D.; Tomney, M. R.; Pye, C. C. *Phys. Chem. Chem. Phys.* **2004**, *6*, 5145–5155.

(47) Lucovsky, G.; Mantini, M. J.; Srivastava, J. K.; Irene, E. A. *J. Vac. Sci. Technol. B Microelectron. Nanom. Struct.* **2000**, *530*, 530–537.

(48) Kamunde-Devonish, M. K.; Fast, D. B.; Mensinger, Z. L.; Gatlin, J. T.; Zakharov, L. N.; Dolgos, M. R.; Johnson, D. W. *Inorg. Chem.* **2015**, *54*, 3913–3920.

(49) Edwards, D. D.; Folkins, P. E.; Mason, T. *J. Am. Ceram. Soc.* **1997**, *80*, 253–257.

(50) Patzke, G.; Binnewies, M. *Solid State Sci.* **2000**, *2*, 689–699.

(51) Lin, W.-T.; Ho, C.-Y.; Wang, Y.-M.; Wu, K.-H.; Chou, W.-Y. *J. Phys. Chem. Solids* **2012**, *73*, 948–952.

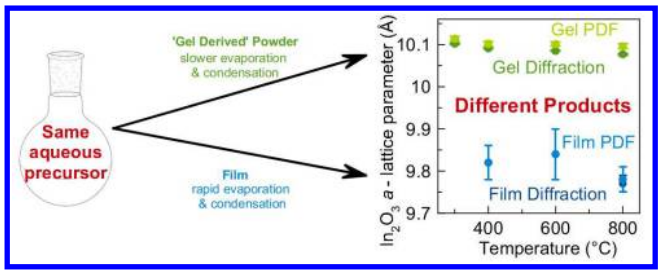
'Gel Derived' Powder
slower evaporation
& condensation
Same
aqueous
precursor
Film
rapid evaporation
& condensation
Gel PDF
Gel Diffraction
Different Products
Film PDF
Film Diffraction
In_2O_3 a - lattice parameter (Å)
10.1
10
9.9
9.8
9.7
400
600
800
Temperature (°C)